A MULTIBAND GENERALIZATION OF THE MULTIHARMONIC ANALYSIS OF VARIANCE PERIOD ESTIMATION ALGORITHM AND THE EFFECT OF INTER-BAND OBSERVING CADENCE ON PERIOD RECOVERY RATE

N. MONDRIK[1,2], J. P. LONG[3], AND J. L. MARSHALL[1]
[1] George P. and Cynthia Woods Mitchell Institute for Fundamental Physics and Astronomy and Department of Physics and Astronomy,
Texas A&M University, College Station, TX 77843-4242, USA; nmondrik@g.harvard.edu
[2] Department of Physics, Harvard University, Cambridge, MA 02138, USA
[3] Department of Statistics Texas A&M University, 3143 TAMU, College Station, TX 77843-3143, USA

ABSTRACT

We present a new method of extending the single-band multiharmonic analysis of variance period estimation algorithm to multiple bands. We use Sloan Digital Sky Survey Stripe 82 RR Lyrae to show that in the case of a low number of observations per band and non-simultaneous observations, improvements in period recovery rates of up to ≈50% are observed. We also investigate the effect of inter-band observing cadence on period recovery rates. We find that using non-simultaneous observation times between bands is ideal for the multiband method, and using simultaneous multiband data is only marginally better than using single-band data. These results will be particularly useful in planning observing cadences for wide-field astronomical imaging surveys such as Large Synoptic Survey Telescope. They also have the potential to improve the extraction of transient data from surveys with few ($\lesssim$30) observations per band across several bands, such as the Dark Energy Survey.

Key words: methods: data analysis – stars: variables: general – stars: variables: RR Lyrae – surveys

1. INTRODUCTION

The period–luminosity relationship of variable stars, first discovered by Henrietta Leavitt and calibrated by Ejnar Hertzsprung (Hertzsprung 1913), is an important step in the astronomical distance ladder. With applications for measuring the Hubble constant (Riess et al. 2011) and mapping out Galactic substructure (Sesar et al. 2010), periodic variables are key science drivers for next-generation astronomical imaging surveys such as the Large Synoptic Survey Telescope (LSST; Ivezić et al. 2008) and *Gaia* (Eyer et al. 2015). Approximately 50 million variable stars will be detected by LSST (Sesar et al. 2007) and 18 million variables by *Gaia* (Eyer & Cuypers 2000); therefore, automated classifiers must be relied upon to find the variable sources and determine the period of the source, if it is periodic.

Numerous period-finding algorithms have been implemented over the years (see Graham et al. 2013 for a comparison of various algorithms). One common characteristic of most modern period-finding algorithms is the use of observational data in a single band. For current generation transient surveys such as the intermediate Palomar Transient Factory (10–5000 observations in *R* band for certain fields[4]; Law et al. 2009) and Optical Gravitational Lensing Experiment (400–500 observations in the *I* band for LMC objects; e.g., Udalski et al. 1992; Soszyński et al. 2009a, 2009b), the volume of data in any one band is sufficient to accurately determine the period, rendering the use of additional bands redundant. However, in multiband surveys in which only a limited number of observations are available in each band, single-band algorithms can struggle due to poor phase coverage (Graham et al. 2013).

Multiband period-finding methods have been explored before, but the proposed methods require either simultaneous measurements (Süveges et al. 2012) or require that a period be correctly recovered by a single-band algorithm in the majority of bands sampled (Oluseyi et al. 2012). The former case puts strict requirements on observing strategy, while the latter still suffers from the inability of single-band algorithms to return accurate results with limited observations. Only recently (Long et al. 2014; VanderPlas & Ivezić 2015) have methods been proposed that are general in the sense of allowing arbitrary observation times and fully incorporating data from multiple bands into an algorithm.

In this Letter, we propose a method to extend the multiharmonic analysis of variance (AoV; Schwarzenberg-Czerny 1996) single-band algorithm to multiple bands. The method improves period recovery rates for poorly sampled multiband light curves. In addition, we discuss the importance of observational cadence between the bands to be used, and we show that non-simultaneous observations between bands increases the ability of our multiband algorithm to recover the correct period.

2. DATA

In this Letter, we select a sample from the 483 RR Lyrae stars from Sesar et al. (2010) and use light curves from the Sloan Digital Sky Survey (SDSS) Stripe 82 Variable Source Catalog (Ivezić et al. 2007). These stars have a reasonably large number of observations, with a median number of observations per band of 56 across the SDSS *g*, *r*, and *i* bands and 55 in *u* and *z*. The data span 3340 days. Of the 483 sources found in Sesar et al. (2010), 33 were either not found in the Variable Source Catalog or had <10 observations in one or more bands. Table 1 gives a complete description of the number of RR Lyrae as a function of the number of observations and the downsampling method (described in Section 3.2). The three band sample uses only the *g*, *r*, and *i* bands. It should also be noted that the typical time for SDSS to complete one pass through all filters is ≈0.004 days (5.7 minutes; York et al. 2000).

---

[4] http://www.ptf.caltech.edu/page/first_data_release

Table 1
Number of RR Lyrae in the Sample

n_{obs} per Band	Non-simulta-neous 5 Band	Simultaneous 5 Band	Non-simulta-neous 3 Band	Simultaneous 3 Band
10	450	450	450	450
13	450	449	450	450
15	450	448	450	449
17	448	447	448	448
19	448	445	448	447
21	447	445	447	445
23	445	440	445	443
25	444	438	444	441

3. METHOD

3.1. Multiharmonic AoV Multiband Extension

As our model for the variation of brightness with time in a single band, we adopt a sinusoid with K harmonics. Assuming n_b observations in each of band b, our data are of the form $\{(t_{bi}, m_{bi}, \sigma_{bi})_{i=1}^{n_b}\}_{b=1}^{B}$, where t_{bi} is the time of the ith observation in band b, m_{bi} is the measured magnitude at that time, and σ_{bi} is the uncertainty associated with m_{bi}. We assume ω, the frequency, is constant across all bands. Our model can be written as

$$
\begin{aligned}
m_{bi} &= \beta_{0b} + \sum_{k=1}^{K} a_{bk} \sin(k\omega t_{bi} + \phi_{bk}) + \epsilon_{bi} \\
&= \beta_{0b} + \sum_{k=1}^{K} \big(a_{bk}\cos(\phi_{bk})\sin(k\omega t_{bi}) \\
&\quad + a_{bk}\sin(\phi_{bk})\cos(k\omega t_{bi})\big) + \epsilon_{bi}
\end{aligned}
\tag{1}
$$

where $\epsilon_{bi} \sim N(0, \sigma_{bi}^2)$ are independent across i and b. This model is equivalent to the multiphase $N_{\mathrm{base}} = 0$, $N_{\mathrm{band}} = K$ model of VanderPlas & Ivezić (2015). The periodogram we construct (see Equation (5), this article) is different than that of VanderPlas & Ivezić (2015). See Equation (5) and the discussion in Section 5 for more details. Long et al. (2014) studied this model with $K = 1$ and termed it MGLS. The authors did not construct periodograms for MGLS and did not study the effects of inter-band observing cadence on period recovery.

One natural approach for estimating ω is to use maximum likelihood. Let $\boldsymbol{a}_b = (a_{b1}, \ldots, a_{bK})$ and $\boldsymbol{a} = (\boldsymbol{a}_1, \ldots \boldsymbol{a}_B)$. Analogous definitions apply for ϕ_b and ϕ. Let $\boldsymbol{\beta}_0 = (\beta_{01}, \ldots, \beta_{0B})$. Since the error model is normal, maximum likelihood is equivalent to finding the ω, which minimizes the weighted sum of squares, sometimes known as "chi-squared minimization."

$$
\begin{aligned}
\widehat{\omega} &= \operatorname*{argmin}_{\omega} \min_{\boldsymbol{a},\phi,\beta_0} \sum_{b=1}^{B}\sum_{i=1}^{n_b} \\
&\quad \left(\Big(m_{bi} - \sum\big(a_{bk}\cos(\phi_{bk})\sin(k\omega t_{bi})\right. \\
&\quad \left. + a_{bk}\sin(\phi_{bk})\cos(k\omega t_{bi})\big) - \beta_{0b}\Big)\Big/(\sigma_{bi})\right)^2 \\
&= \operatorname*{argmin}_{\omega} \sum_{b=1}^{B} \min_{\boldsymbol{a}_b,\phi_b,\beta_{0b}} \sum_{i=1}^{n_b} \\
&\quad \left(\Big(m_{bi} - \sum\big(a_{bk}\cos(\phi_{bk})\sin(k\omega t_{bi})\right. \\
&\quad \left. + a_{bk}\sin(\phi_{bk})\cos(k\omega t_{bi})\big) - \beta_{0b}\Big)\Big/(\sigma_{bi})\right)^2 .
\end{aligned}
$$

We moved the min inside the sum over b because the bth summand only depends on $\boldsymbol{a}_b$, ϕ_b, β_{0b}.

The sum over i can be simplified by noting the linearity of the model and reparameterizing. Let $\boldsymbol{m}_b = (m_{b1}, \ldots, m_{bn_b})^T$. Let $\beta_{bk1} = a_{bk}\cos(\phi_{bk})$ and $\beta_{bk2} = a_{bk}\sin(\phi_{bk})$. Define $\boldsymbol{\beta}_b = (\beta_{0b}, \beta_{b11}, \beta_{b12}, \ldots, \beta_{bK1}, \beta_{bK2})^T \in \mathbb{R}^{2K+1}$. Let $\boldsymbol{\Sigma}_b$ be a $n_b \times n_b$ diagonal matrix where $\Sigma_{bii} = \sigma_{bi}^2$. Define

$$
\begin{aligned}
&\boldsymbol{X}_b(\omega) \\
&= \begin{pmatrix}
1 & \sin(\omega t_{b1}) & \cos(\omega t_{b1}) & \ldots & \sin(K\omega t_{b1}) & \cos(K\omega t_{b1}) \\
1 & \sin(\omega t_{b2}) & \cos(\omega t_{b2}) & \ldots & \sin(K\omega t_{b2}) & \cos(K\omega t_{b2}) \\
\vdots & \vdots & \vdots & \ddots & \vdots & \vdots \\
1 & \sin(\omega t_{bn_b}) & \cos(\omega t_{bn_b}) & \ldots & \sin(K\omega t_{bn_b}) & \cos(K\omega t_{bn_b})
\end{pmatrix} \\
&\in \mathbb{R}^{n_b \times (2K+1)}.
\end{aligned}
$$

We rewrite the ML estimator as

$$
\widehat{\omega} = \operatorname*{argmin}_{\omega} \sum_{b=1}^{B} \min_{\boldsymbol{\beta}_b} \big(\boldsymbol{m}_b - \boldsymbol{X}_b(\omega)\boldsymbol{\beta}_b\big)^T \boldsymbol{\Sigma}_b^{-1} \big(\boldsymbol{m}_b - \boldsymbol{X}_b(\omega)\boldsymbol{\beta}_b\big).
$$

The problem is now identical to weighted least squares, so the $\boldsymbol{\beta}_b$ that minimizes the expression is

$$
\widehat{\boldsymbol{\beta}}_b(\omega) = \big(\boldsymbol{X}_b^T(\omega)\boldsymbol{\Sigma}_b^{-1}\boldsymbol{X}_b(\omega)\big)^{-1}\boldsymbol{X}_b(\omega)^T\boldsymbol{\Sigma}_b^{-1}\boldsymbol{m}_b.
$$

Define

$$
\mathrm{RSS}_b(\omega) = \big(\boldsymbol{m}_b - \boldsymbol{X}_b(\omega)\widehat{\boldsymbol{\beta}}_b(\omega)\big)^T \boldsymbol{\Sigma}_b^{-1}\big(\boldsymbol{m}_b - \boldsymbol{X}_b(\omega)\widehat{\boldsymbol{\beta}}_b(\omega)\big)
\tag{2}
$$

and we have

$$
\widehat{\omega} = \operatorname*{argmin}_{\omega} \sum_{b=1}^{B}\mathrm{RSS}_b(\omega).
\tag{3}
$$

One can reconstruct maximum likelihood estimators for the original parameterization from the $\widehat{\boldsymbol{\beta}}_b(\widehat{\omega})$. From a computational perspective, the ML estimator requires performing B weighted least squares estimates at each frequency.

Rather than obtain a single period estimate, it may be useful at any proposed ω to have a measure of the confidence that ω is the true frequency. Periodograms are functions that map frequencies to some measure of confidence. Often periodograms are constructed so that under the null hypothesis of no magnitude variation (i.e., $m_{bi} = \beta_{b0} + \epsilon_{bi}$), the periodogram has a known distribution at any particular frequency. We construct such a periodogram for the model specified by Equation (1). The frequency that maximizes this periodogram will be shown to be the maximum likelihood estimator in Equation (3). This periodogram is a direct generalization of the AoV periodogram of Schwarzenberg-Czerny (1996) to multiband data because:

1. With a single band, the periodogram simplifies to the AoV periodogram of Schwarzenberg-Czerny (1996).
2. The periodogram retains the F distribution under the null hypothesis of constant magnitude in every band.

We now discuss how to construct the periodogram following the notation of Section 3.1. We then go into further detail regarding the equivalence of this periodogram to Schwarzenberg-Czerny (1996) and compare this periodogram to VanderPlas & Ivezić (2015).

Under the notation of the previous section, the model in Equation (1) can be written as

$$\boldsymbol{m}_b = \boldsymbol{X}_b(\omega)\boldsymbol{\beta}_b + \boldsymbol{\epsilon}_b \qquad (4)$$

where $\boldsymbol{\epsilon}_b \sim N(0, \boldsymbol{\Sigma}_b)$ for all b. Consider testing the null hypothesis

$$H_0 : \boldsymbol{m}_b = 1\beta_{b0} + \boldsymbol{\epsilon}_b \ \forall \ b.$$

This hypothesis states that the magnitude is a constant β_{b0} in each band. Since the first column of $\boldsymbol{X}_b(\omega)$ is $\boldsymbol{1}$, this is a submodel of Equation (4). The weighted least squares estimator for the submodel is

$$\widehat{\beta}_{b0} = \left(1^T \boldsymbol{\Sigma}_b^{-1} 1\right)^{-1} 1^T \boldsymbol{\Sigma}_b^{-1} \boldsymbol{m}_b = \frac{1}{\sum_{i=1}^{n_b} \sigma_{bi}^{-2}} \sum_{i=1}^{n_b} \frac{m_{bi}}{\sigma_{bi}^2}.$$

The residual sum of squares is

$$\mathrm{RSS}_b^0 = \left(\boldsymbol{m}_b - 1\widehat{\beta}_{b0}\right)^T \boldsymbol{\Sigma}_b^{-1} \left(\boldsymbol{m}_b - 1\widehat{\beta}_{b0}\right).$$

Standard results in statistics (for example, Sections 2.5 and 2.6 of Scheffé 1959) show that under the null hypothesis

$$\mathrm{RSS}_b^0 - \mathrm{RSS}_b(\omega) \sim \chi^2_{2K}$$
$$\mathrm{RSS}_b(\omega) \sim \chi^2_{n_b - 2K - 1}$$

where χ^2_j refers to a chi-squared distribution with j degrees of freedom. Further, these two quantities are independent. Since the sum of χ^2 random variables is χ^2, we have

$$\sum_{b=1}^B \mathrm{RSS}_b^0 - \sum_{b=1}^B \mathrm{RSS}_b(\omega) \sim \chi^2_{2KB}$$
$$\sum_{b=1}^B \mathrm{RSS}_b(\omega) \sim \chi^2_{\sum_{b=1}^B n_b - 2KB - B}.$$

Finally, we define the periodogram at frequency ω to be the ratio of these quantities divided by their respective degrees of freedom

$$\Theta(\omega) = \frac{\left(\sum_{b=1}^B n_b - 2KB - B\right)\left(\sum_{b=1}^B \mathrm{RSS}_b^0 - \sum_{b=1}^B \mathrm{RSS}_b(\omega)\right)}{2\, KB \left(\sum_{b=1}^B \mathrm{RSS}_b(\omega)\right)}. \qquad (5)$$

Under H_0, $\Theta(\omega) \sim F_{2\, KB, \sum_{b=1}^B n_b - 2KB - B}$. A few comments on the periodogram:

1. In practice, the frequency that maximizes the periodogram is often used as a period estimate. The frequency that maximizes the periodogram will minimize $\sum_{b=1}^B \mathrm{RSS}_b(\omega)$, which we showed in Equation (3) is the maximum likelihood estimator.

2. With a single band, the periodogram becomes

$$\Theta(\omega) = \frac{(n - 2K - 1)\left(\mathrm{RSS}^0 - \mathrm{RSS}(\omega)\right)}{2K\left(\mathrm{RSS}(\omega)\right)}$$

which matches the periodogram of Schwarzenberg-Czerny (1996, Equation (11)).

In addition to developing the single-band AoV algorithm, Schwarzenberg-Czerny (1996) also developed a fast routine for evaluating $\mathrm{RSS}_b(\omega)$ based on finding orthogonal polynomials on the unit circle. For this reason, we use a Fortran

implementation of the single-band AoV algorithm[5] as the basis for constructing our multiband periodogram. A small python code demonstrating how to do this been made available.[6] As input parameters to the single-band AoV algorithm used in this work, we use a minimum frequency of 1 day^{-1}, an upper frequency of 5 day^{-1}, a frequency step of 0.0001 day^{-1}, and one harmonic (corresponding to FR0 = 1, FRU = 5, FRS = 0.0001, and NH2 = 2 in the AoV code).

This periodogram is different from that of VanderPlas & Ivezić (2015; see Equation (22) in their paper). They use RSS_b^0 in the denominator instead of $\mathrm{RSS}_b(\omega)$. The unregularized models of VanderPlas & Ivezić (2015) follow an incomplete beta distribution (see Schwarzenberg-Czerny 1998, Equation (6)). It should also be noted that our multiband method implicitly assumes that the period of oscillation is the same for each band. If the period varies significantly across bands, this method will not be suitable for use.

Figure 1 compares the multiband periodogram with its single-band counterparts.

3.2. Testing the Algorithm

To test the algorithm, we downsample the number of observations per band for each light curve using both simultaneous and non-simultaneous downsampling. For non-simultaneous downsampling, observations (consisting of a time of observation, band, magnitude, and photometric error) are randomly selected from all available observations. Observations are selected until all bands have n_{obs} observations. For simultaneous downsampling, an observation in one band is chosen. We then choose observations in the other bands such that the absolute difference in observation times is $\leqslant 0.005$ days (7.2 minutes) from the initial observation time. This is repeated n_{obs} times. Since the time for SDSS to complete one pass through all filters is about 5.7 minutes (York et al. 2000), these observations are as close in phase space as possible. We also choose to use a flat time difference rather than a fraction of the known period in order to mimic the lack of a priori knowledge of the variable object, as is the case in survey planning. We then define a period as correctly recovered if $|P_{\mathrm{Alg}} - P_{\mathrm{True}}| \leqslant 0.001$ days, where P_{Alg} is the period corresponding to the largest value of the multiband or single-band AoV periodogram, and P_{True} is the period as measured by Sesar et al. (2010). The results are shown in Figure 2. Error bars are estimated by assuming a binomial distribution at each n_{obs} characterized by the estimated completeness and number of objects.

4. DISCUSSION

4.1. Benefit of Multiband over Single Band

The most striking result shown in Figure 2 is the large separation between the multiband non-simultaneous completeness fraction and the single-band non-simultaneous completeness fraction; even the use of as few as 3 bands can significantly improve recovery rates over single-band methods. For surveys with a low number of observations per band ($n_{\mathrm{obs}} \lesssim 30$), such as the Dark Energy Survey (The Dark Energy Survey Collaboration 2005), multiband methods can provide a significant increase in fraction of correctly recovered periods,

---

5　http://users.camk.edu.pl/alex/
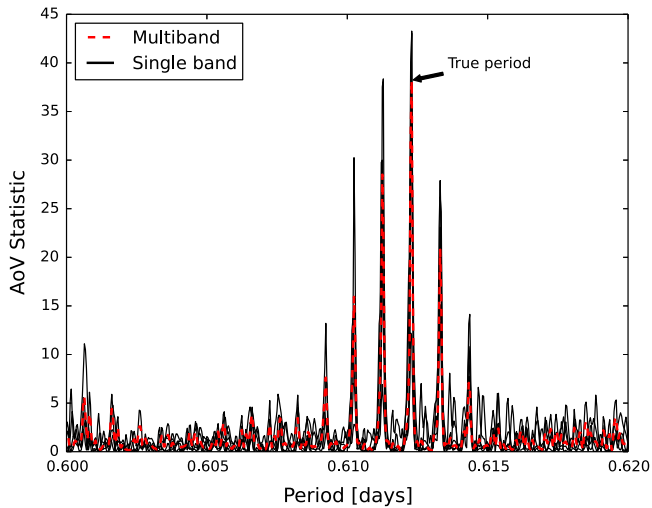6　https://github.com/Mondrik/Multiband_AoV_Demo

Figure 1. Single-band AoV periodograms and multiband periodogram constructed using Equation (5). The AoV statistic is an indication of how well the trial function of the AoV algorithm fits the light curve folded with period P, with higher values indicating a better fit. The multiband periodogram is given by the red dashed line, while the *ugriz* single-band periodograms are given by the solid black lines. The periodogram was generated using non-simultaneous downsampling (to 19 observations per band in 5 bands) of an RR Lyrae from Sesar et al. (2010).

Figure 2. Completeness fraction (number of periods correctly recovered divided by number of light curves attempted, period is successfully recovered if $|P_{Alg} - P_{True}| \leqslant 0.001$ days) as a function of observations per band across the SDSS *ugriz* bands. The 483 RR Lyrae of Sesar et al. (2010) were used as a data set, as described in Section 2. Single-band periods and one multiband period were estimated for each object. The single-band completeness is obtained by dividing the number of correct single-band period identifications by the total number of single-band light curves attempted (i.e., 5x, 3x, or 1x the number of RR Lyrae), while multiband completeness is calculated by dividing the number of multiband correct period identifications by the number of RR Lyrae attempted. The solid (dashed) black line with circles represent the completeness fraction for 5 band (*ugriz*) non-simultaneous (simultaneous) downsampling. The green solid (dashed) lines and star markers are the same, but for 3 bands (*gri*) of data. The single-band counterparts for non-simultaneous and simultaneous downsampling are given by the solid red line and dashed blue line with triangles, respectively. For simultaneous observations, the typical separation between observations is $\lesssim 0.005$ days.

allowing for more accurate classification of transient objects in the survey.

4.2. Impact of Inter-band Observing Cadence

The second major result noticeable in Figure 2 is the difference between the simultaneous and non-simultaneous downsampling groups. It should be noted that in the single-band case, simultaneous and non-simultaneous downsampling should have no effect, so the scatter between the two is indicative of the randomness in choosing the observations. The difference between multiband non-simultaneous and simultaneous downsampling arises primarily from the increase in phase-space coverage of the non-simultaneous downsampling relative to the simultaneous downsampling. In the case of simultaneous downsampling, the additional bands add little new information about the light curve not contained in other bands, leading to poorer performance, despite having the same number of total observations.

Figure 3 demonstrates the failure modes of our multiband model in the case of non-simultaneous and simultaneous observations. We plot the best-fit period from the AoV multiband model with 15 observations per band against the period taken from Sesar et al. (2010). In the non-simultaneous case, the multiband method fails primarily along beat periods, given by $P_n = P/(1 + nP)$ for integer n, as discussed in VanderPlas & Ivezić (2015). In the simultaneous case, the multiband method tends to fail in a much more random fashion.

4.3. Constructing Data Sets for Maximized Period Recovery Rates

The improvement of recovery rates with unique phase-space observations (non-simultaneous observations) suggests that recovery rates cannot be significantly improved by down-sampling 25 simultaneous observations to, for example, sets of 12 observations that are less simultaneous. Fundamentally, there are only 25 unique phase-space observations of the
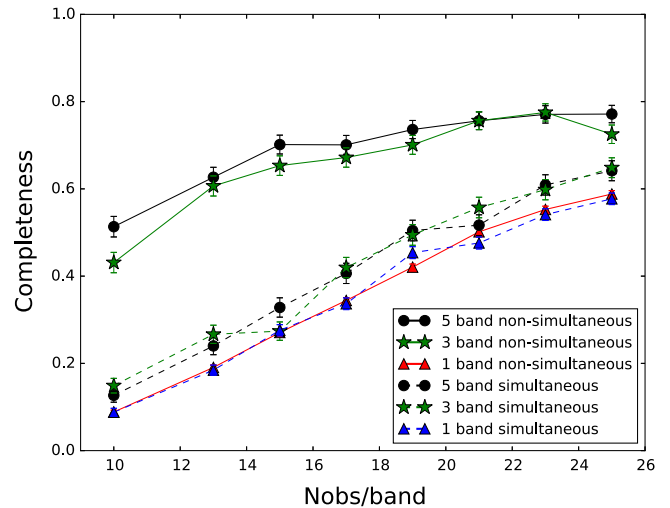
object, which constrains the maximum amount of phase-space separation between the bands. In order to construct a truly non-simultaneous data set, we require a minimum of n_{obs} per band times the number of bands. Hence, our non-simultaneous downsampling set is not truly non-simultaneous since we are randomly downsampling from less than 125 observations across 5 bands (at 25 observations per band). Since the typical number of observations per band is ≈ 55, it is impossible for us to separate the observations completely for $n_{obs} > 11$ in 5 bands. In this case, the algorithm is limited by the construction of the data set, i.e., how non-simultaneous the observations are. It would therefore be advantageous to construct a data set that is as non-simultaneous as possible, rather than downsample from a simultaneous data set, in order to use the maximum number of observations.

4.4. Implications for Future Imaging Surveys

This method of constructing a data set has a major potential impact on observational cadence planning for upcoming wide-field imaging surveys such as LSST. By varying observation times between bands, accurate periods for variable sources can be estimated much sooner than otherwise possible. The phase-space effect also has implications for our ability to extract transient data from ongoing surveys such as the Dark Energy Survey, which could see a boost in period recovery rates by employing an algorithm similar to our proposed method.
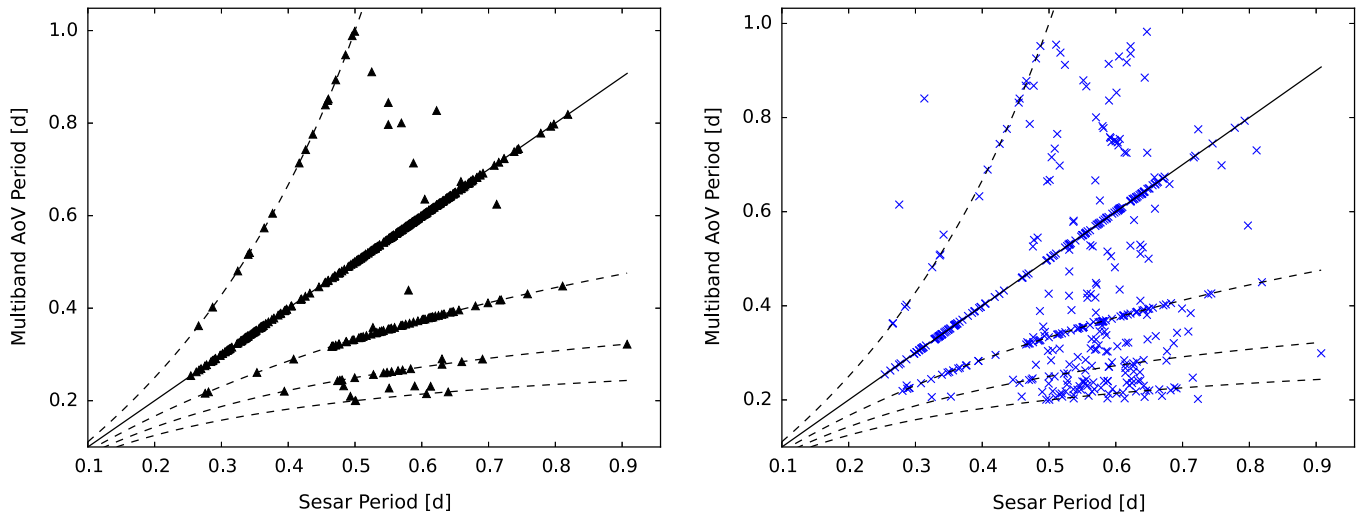
Figure 3. Comparison of best-fit periods from this work to Sesar et al. (2010) for the multiband method in the non-simultaneous (left) and simultaneous (right) cases. Periodograms were made using 15 observations per band. The solid line represents a 1:1 match, while the dashed lines represent beat frequencies. In general, the non-simultaneous data set fails along beat frequencies, while the simultaneous data set fails in a more random manner.

5. COMPARISON WITH VANDERPLAS AND IVEZIĆ (2015)

As we mentioned earlier, another method similar to ours in spirit is that of VanderPlas & Ivezić (2015). Both methods use truncated Fourier series to model given observations across an arbitrary number of bands. However, the method used in VanderPlas & Ivezić (2015) is effectively an extension of the Lomb–Scargle periodogram (Lomb 1976; Scargle 1982), while ours extends the AoV periodogram. Schwarzenberg-Czerny (1998) asserts that statistically the use of PDM (Jurkevich 1971; Stellingwerf 1978), AoV, and χ^2 statistics is largely a matter of taste, although it will be interesting to perform another analysis similar to that of Graham et al. (2013) on multiband data using methods such as ours and that of VanderPlas & Ivezić (2015) to determine when each algorithm is most effective.

6. CONCLUSION

We have introduced a new method of estimating periods of periodic variables using multiband imaging data. We extended the existing AoV period estimation algorithm to incorporate data from multiple bands while maintaining the fundamental characteristics of the single-band algorithm. This allows for the use of relatively few observations (≈ 25) per band across several bands while maintaining a reasonable level of completeness ($\approx 70\%$–80%). We have also shown the importance of the (non-)simultaneity of observation timing. For a fixed number of observations per band, non-simultaneous observations offer better opportunity for period recovery than simultaneous observations. This effect of observational simultaneity has implications for the area of survey planning, particularly in the early period of surveys such as LSST, when the volume of data is not enough to render multiband period estimation redundant. It also has implications for non-transient surveys imaging fields at multiple epochs. By carefully choosing the observation time and band, our proposed mutiband algorithm can extract periods from data previously considered too poorly sampled to be of use.

REFERENCES

Eyer, L., & Cuypers, J. 2000, in ASP Conf. Ser. 203, IAU Coll. 176: The Impact of Large-Scale Surveys on Pulsating Star Research, ed. L. Szabados & D. Kurtz (San Francisco, CA: ASP), 71
Eyer, L., Rimoldini, L., Holl, B., et al. 2015, arXiv:1502.03829
Graham, M. J., Drake, A. J., Djorgovski, S. G., et al. 2013, MNRAS, 434, 3423
Hertzsprung, E. 1913, AN, 196, 201
Ivezić, Ž., Smith, J. A., Miknaitis, G., et al. 2007, AJ, 134, 973
Ivezić, Ž., Tyson, J. A., Abel, B., et al. 2008, arXiv:0805.2366
Jurkevich, I. 1971, Ap&SS, 13, 154
Law, N. M., Kulkarni, S. R., Dekany, R. G., et al. 2009, PASP, 121, 1395
Lomb, N. R. 1976, Ap&SS, 39, 447
Long, J. P., Chi, E. C., & Baraniuk, R. G. 2014, arXiv:1412.6520
Oluseyi, H. M., Becker, A. C., Culliton, C., et al. 2012, AJ, 144, 9
Riess, A. G., Macri, L., Casertano, S., et al. 2011, ApJ, 730, 119
Scargle, J. D. 1982, ApJ, 263, 835
Scheffé, H. 1959, The Analysis of Variance (New York: Wiley-Interscience)
Schwarzenberg-Czerny, A. 1996, ApJL, 460, L107
Schwarzenberg-Czerny, A. 1998, MNRAS, 301, 831
Sesar, B., Ivezić, Ž., Grammer, S. H., et al. 2010, ApJ, 708, 717
Sesar, B., Ivezić, Ž., Lupton, R. H., et al. 2007, AJ, 134, 2236
Soszyński, I., Udalski, A., Szymański, M. K., et al. 2009a, AcA, 59, 1
Soszyński, I., Udalski, A., Szymański, M. K., et al. 2009b, AcA, 59, 239
Stellingwerf, R. F. 1978, ApJ, 224, 953
Süveges, M., Sesar, B., Váradi, M., et al. 2012, MNRAS, 424, 2528
The Dark Energy Survey Collaboration 2005, arXiv:astro-ph/0510346
Udalski, A., Szymanski, M., Kaluzny, J., Kubiak, M., & Mateo, M. 1992, AcA, 42, 253
VanderPlas, J. T., & Ivezić, Ž. 2015, arXiv:1502.01344
York, D. G., Adelman, J., Anderson, J. E., Jr., et al. 2000, AJ, 120, 1579